J-9.3 Contribution from CPP-31

The following results are presented to analyze the contribution from CPP-31 for the model predictions presented in Section J-8.

J-9.3.1 Vadose Zone Sr-90 Simulation Results

The spatial distribution of Sr-90 originating at site CPP-31 is shown in Figures J-9-19 through J-9-22. These vadose zone contours include the affects from the initial rapid release of 12336 Ci in addition to the slow release from the alluvium of the residual 3564 Ci. In comparison to the distribution obtained for the Site CPP-79 deep release, (Figures J-9-10 through J-9-13), they are remarkably similar. This similarity occurs because 1) the significant activity released from the alluvium for CPP-31 occurred over a relatively small time frame (0-7 years), followed by an insignificant additional release throughout the remaining time period, and 2) the activity released in CPP-79 was placed just above the basalt-alluvium interface, followed by a relatively large volume of water just above the source location. In the case of CPP-31, the initial mobile activity is on the order of 12336 Ci, and in the case of CPP-79 deep, the activity is about 1000 Ci. The release history accounts for the similarity in time required to reach the perched water, and close release locations at land surface account for much of the spatial similarity. The vertical distribution of Sr-90 from Site CPP-31 in year 1979 extends from land surface to the aquifer. This very early arrival of Sr-90 in relatively high pore water concentrations is a result of dispersive transport. Even though the vertical profiles suggest that flow is primarily vertical, the horizontal contour plots show that the lateral extent impacted by CPP-31 is extensive.

Peak vadose zone concentrations for the CPP-31 source through time are shown in black in Figure J-9-23 and are slightly below 10,000 pCi/L in year 2300. The three separate arrivals of Sr-90 in the vadose zone are a reflection of the relative mobility of SrNO3, Sr+ ion, and SrOH. Peak concentrations in the vadose zone for the RI/BRA base case (black) and those from this simulation are nearly identical and are a reflection of the pore water concentration in the alluvium.

The rate at which this activity enters the aquifer is given in Figure J-9-24 (shown in red), and can be compared directly to the RI/BRA model including all of the sources (shown in black). Compared to the flux originating from site CPP-79, it is apparent that most of the post 2000 contribution will have originated from site CPP-31. In consideration of the results shown in Section J-9.4, it is clear that this activity originated with the initial early release from CPP-31, and is not coming from the Sr-90 remaining in the alluvium after 1993.

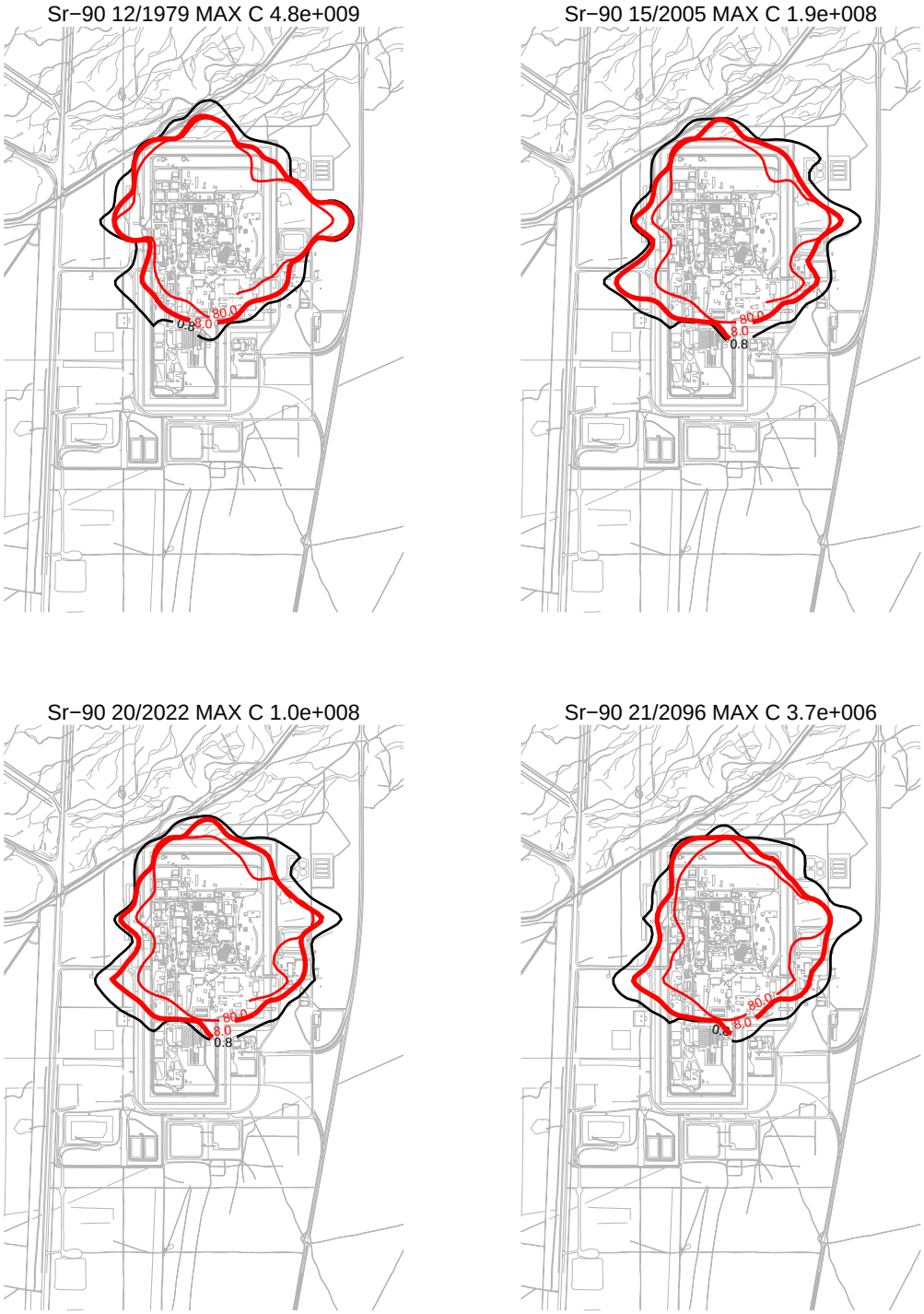

Figure J-9-19. Sr-90 vadose zone concentration from CPP-31 (horizontal contours) (pCi/L) (MCL = thick red line, 10*MCL = thin red line, MCL/10 = black line).

Figure J-9-20. Sr-90 vadose zone concentration from CPP-31 (horizontal contours) (pCi/L) (MCL = thick red line, 10*MCL = thin red line, MCL/10 = black line).

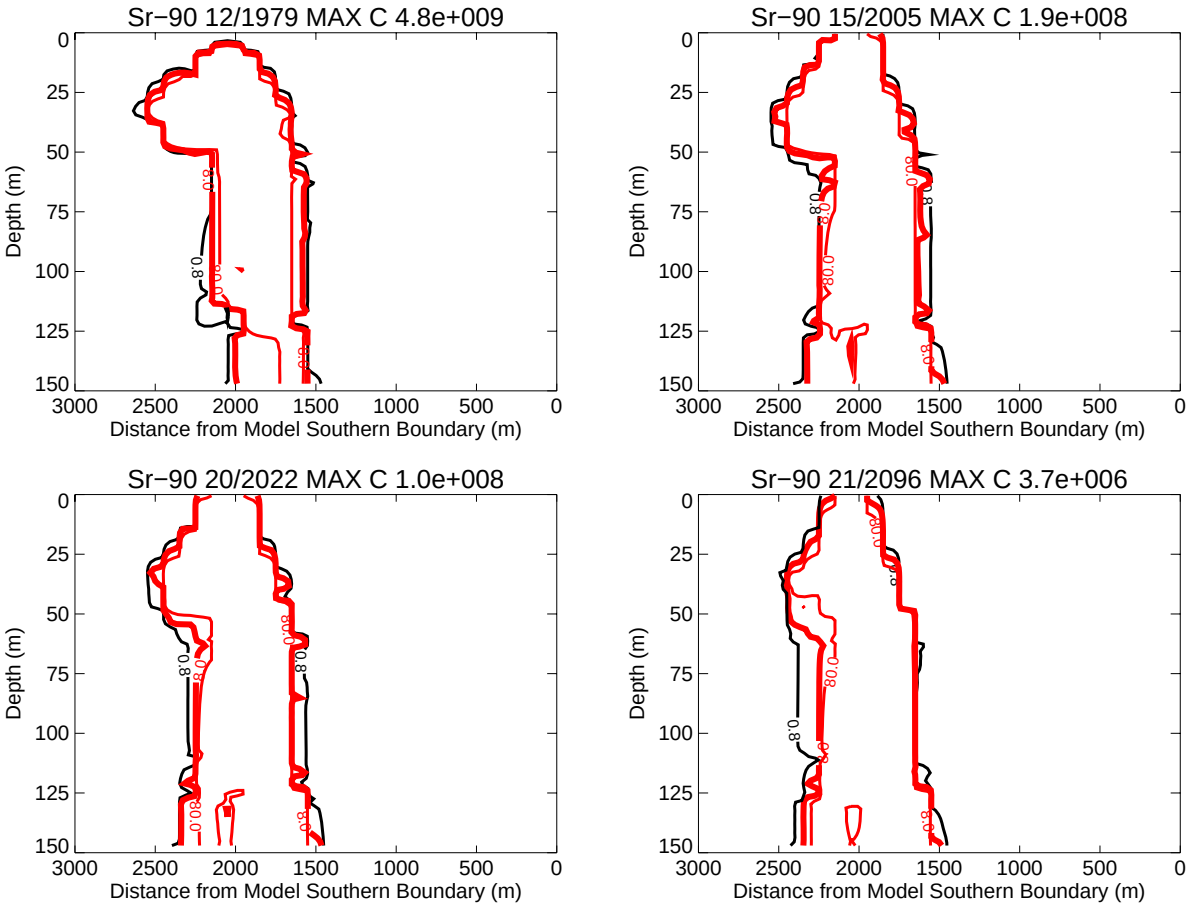

Figure J-9-21. Sr-90 vadose zone concentrations from CPP-31 (vertical contours) (pCi/L) (MCL = thick red line, 10*MCL = thin red line, MCL/10 = black line).

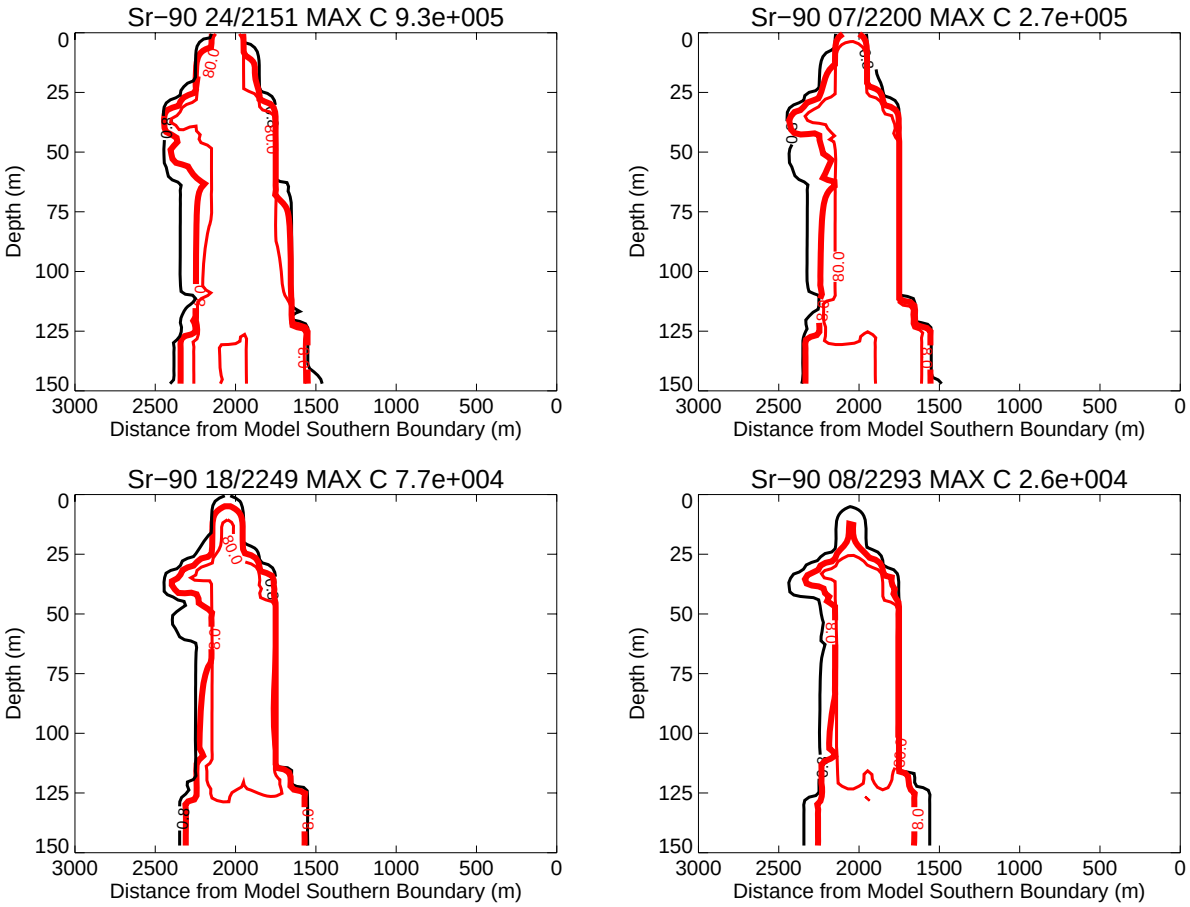

Figure J-9-22. Sr-90 vadose zone concentrations from CPP-31 (vertical contours) (pCi/L) (continued) (MCL = thick red line, 10*MCL = thin red line, MCL/10 = black line).

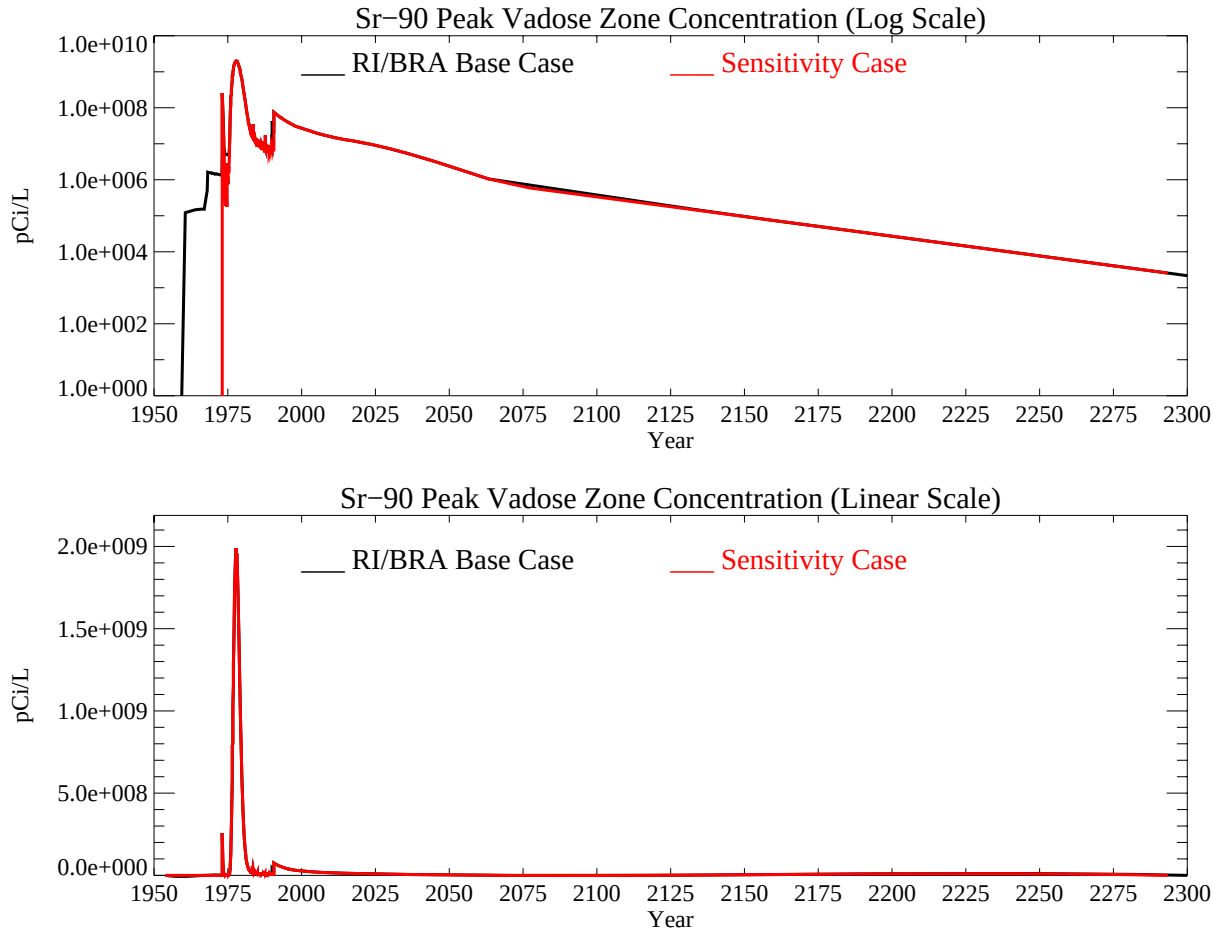

Figure J-9-23. Sr-90 peak vadose zone concentrations from CPP-31 (pCi/L) with the RI/BRA model in black and the CPP-31 source in red.

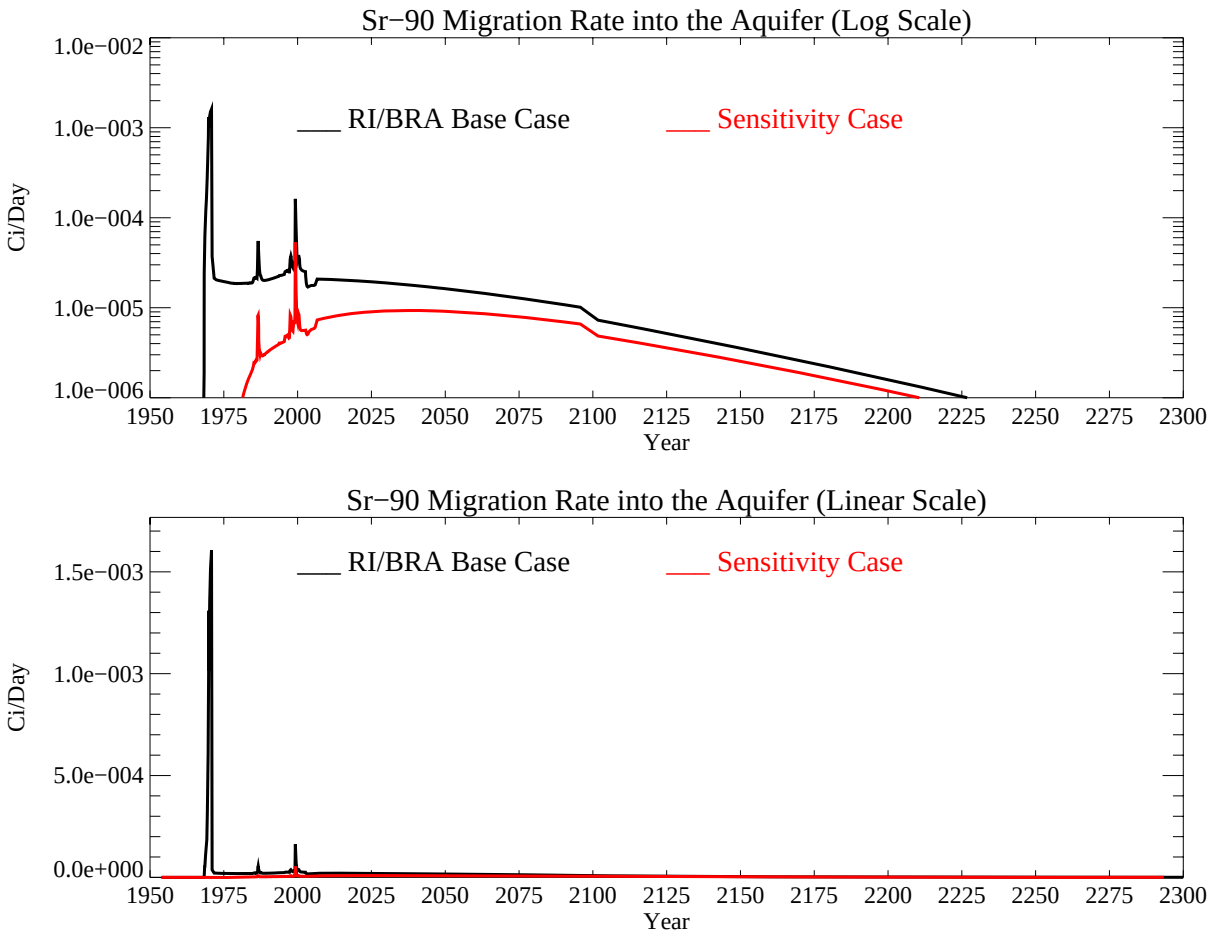

Figure J-9-24. Sr-90 activity flux into the aquifer from CPP-31 (Ci/day) with the RI/BRA model in black, and the CPP-31 source in red.

J-9.3.2 Aquifer Sr-90 Simulation Results

The distribution of Sr-90 in the aquifer for the time period spanning 1979-2096 is given for the far-field in Figure J-9-25. Near-field results representative of the fine-grid are shown for the 2096-2249 time period in Figure J-9-26. The contours for year 2005 indicate that the aquifer is currently being impacted by Site CPP-31. Contours for years 2095-2200 indicate that the highest concentrations occur to the south of INTEC with an extension to the north, consistent with predictions for Tc-99. This differs from the impact of CPP-79 which occurs further south and west. Differences in north-south flow patterns arise as a result of the interbed topology that creates an apparent divide close to directly below INTEC. The area impacted by CPP-31 is considerably smaller than that predicted to be impacted by other Sr-90 sources combined through year 2022, but is larger after year 2096. Sr-90 concentrations are predicted to remain above the MCL during the 1986-2107 time period. This is apparent in the peak aquifer concentration plot given in Figure J-9-27. By comparing the contribution from CPP-79, the impact of CPP-31 is much longer in duration with concentrations predicted to fall below 8 pCi/L for CPP-79 in year 2107.

At a maximum, the highest aquifer impact occurs in the 2000-time frame, with concentrations in the aquifer approaching 61.5 pCi/L. This is larger than the 12.9 pCi/L contribution from CPP-79. In contrast, the predicted peak Sr-90 concentration from CPP-31 in the year 2095 is 4.6 pCi/L, which is about equal to that from CPP-79 and to that from non-CPP-79 and non-CPP-31 sources. The area impacted by CPP-31 above the 0.8 pCi/L level mimics the area impacted above the MCL when all sources were considered in the RI/BRA model. This indicates that the majority of impact at times beyond 2095 is a result of the Sr-90 released into the perched water.

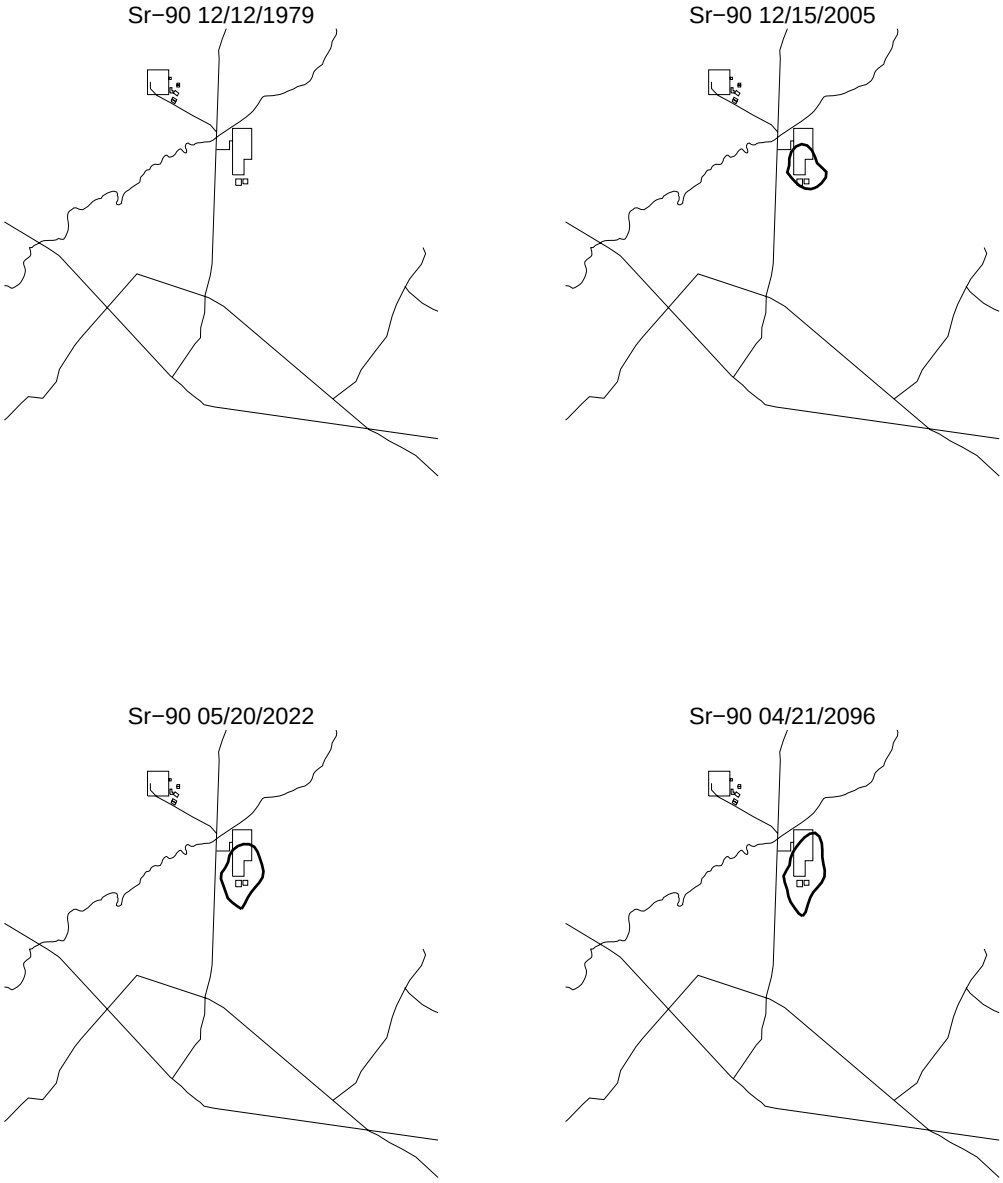

Figure J-9-25. Sr-90 aquifer concentration contours from CPP-31 (pCi/L) (MCL = thick red line, 10*MCL = thin red line, MCL/10 = black line).

Figure J-9-26. Sr-90 aquifer concentration contours from CPP-31 (pCi/L) (continued) (MCL = thick red line, 10*MCL = thin red line, MCL/10 = black line).

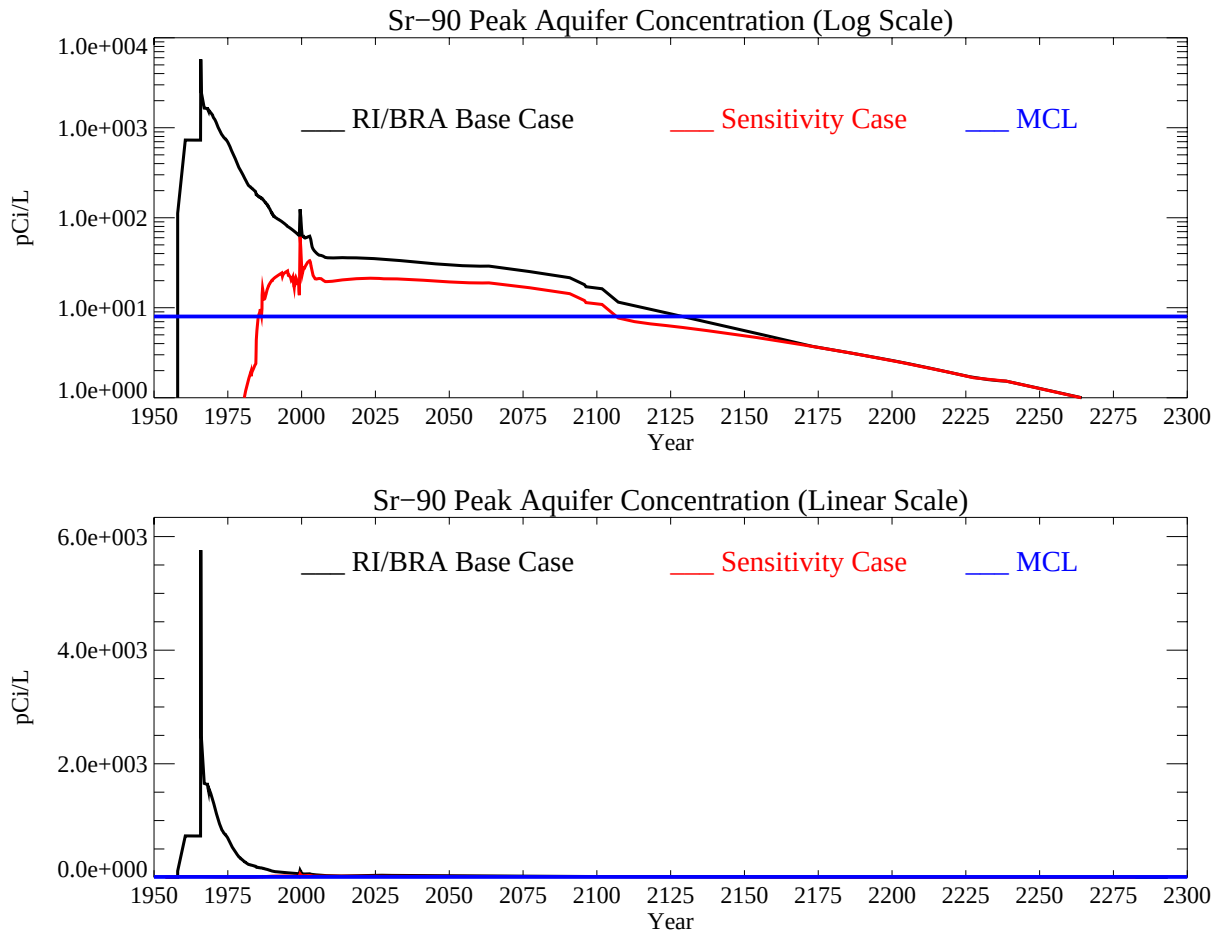

Figure J-9-27. Sr-90 peak aquifer concentrations from CPP-31 (pCi/L) with the MCL in blue, the RI/BRA model in black, and the CPP-31 source in red.

J-9.4 Contribution By Sr-90 Remaining in the Alluvium at CPP-31

In the model results presented in Sections J-8.2, J-8.3, and J-9.3, it was not clear whether or not the Sr-90 thought to remain in the alluvium after year 1992 was contributing significantly to predicted aquifer concentrations. The bulk of this residual Sr-90 would be associated with CPP-31, and would consist of the 3564 Ci distributed throughout the alluvium. It would not include much, if any, of the original 874 Ci from CPP-79 deep because that release occurred just above the alluvium-basalt interface. The later CPP-79 shallow release occurred above CPP-79 deep, contained fewer curies of Sr-90, and was accompanied by 25,000 gallons of water. That later release would have rapidly flushed most of the Sr-90 from CPP-79 deep into the northern upper shallow perched water, leaving very little in the alluvium. The following simulation results evaluate the contribution to aquifer concentrations from the 3564 Ci of Sr-90 thought to remain in the alluvium after year 1972. In this simulation, only the 3564 Ci source was considered.

J-9.4.1 Vadose Zone Sr-90 Simulation Results

In this simulation, 3564 Ci of Sr-90 were distributed vertically in the alluvium in year 1993. As in the RI/BRA base case (considering all sources of Sr-90), this 3564 Ci was distributed vertically through the alluvium, with the activity distribution scaled to the measured soil concentrations obtained during the 2004 sampling (Appendix G, and Table 5-32). This mapping allows most of the activity to be placed at the elevation of the highest measured soil concentrations, with less activity located deeper. To simulate the transport of the activity remaining in the alluvium, an effective K_d of 2 mL/g was used (Figure J-8-9 (J)) for the alluvium sediments.

Figures J-9-28 through J-9-31 illustrate the distribution of Sr-90 in the vadose zone through the year 2293. The concentration isopleths on those plots are for 80., 8.0, and 0.8 pCi/L levels as thin red, thick red, and black lines, respectively. These contours represent the concentration of Sr-90 in the pore water in the alluvium in addition to representing the concentration of Sr-90 in the perched water. The horizontal distribution of Sr-90 in the vadose zone pore water is confined to a much smaller area compared to that obtained considering all of the CPP-31 release (compare Figures J-9-19 and J-9-28). The downward transport allows some Sr-90 to reach the vadose zone-aquifer interface by year 2005 in concentrations just above 8 pCi/L, and by 2096, there is a very small area at this interface where concentrations of 80 pCi/L exist. However, by year 2200, the region above 80 pCi/L has receded upward and is above the 380 ft interbed where it remains through year 2293. After these concentrations reach the aquifer, they will be diluted, and will be much lower than they are predicted to be in the vadose zone.

Peak vadose zone concentrations through time are given in Figure J-9-32. The highest value occurs in 1990, and is 7.5e7 pCi/L. Concentrations are highest in the alluvium, and decrease with depth as the Sr-90 is diluted by influxing water from anthropogenic sources, precipitation infiltration, and from the Big Lost River.

The rate at which this activity enters the aquifer is shown by the red line in Figure J-9-33. For comparison, the rate at which Sr-90 enters the aquifer in the RI/BRA base case is included as the black line. This figure clearly indicates that the flux of Sr-90 entering the aquifer from the residual amount remaining at site CPP-31 in the alluvium is about 10% of that predicted to arrive from other sources. This flux occurs at about 1E-6 Ci/day during a relatively brief period between years 2060 and 2100. This forty year period is much shorter than that the period impacted by the other sources combined. The impact of this relatively small contribution to aquifer concentrations is shown in Figure J-9-34.

Figure J-9-28. SR-90 remaining in the alluvium from CPP-31: vadose zone concentration (horizontal contours) (pCi/L) (MCL = thick red line, 10*MCL = thin red line, MCL/10 = black line).

Figure J-9-29. Sr-90 remaining in the alluvium from CPP-31: vadose zone concentration (horizontal contours) (pCi/L) (MCL = thick red line, 10*MCL = thin red line, MCL/10 = black line).

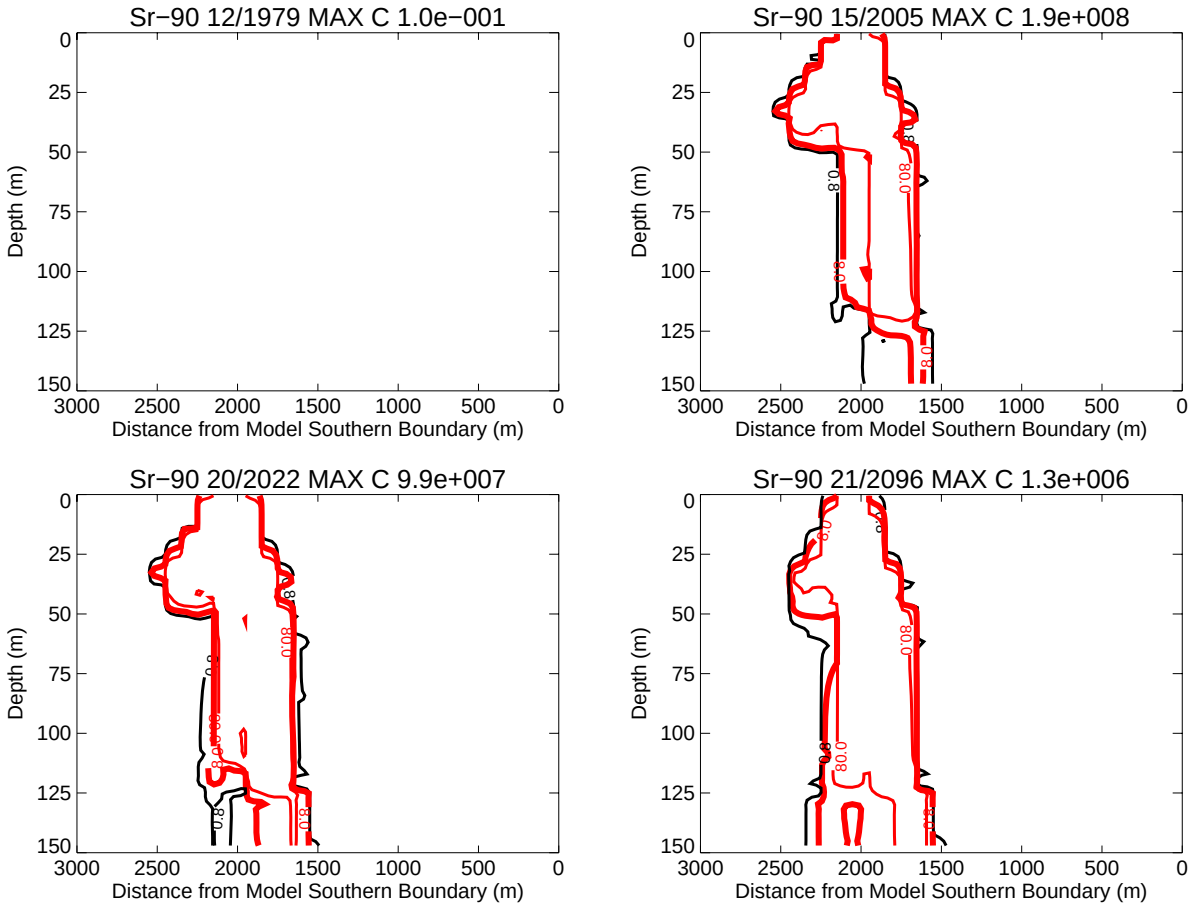

Figure J-9-30. Sr-90 remaining in the alluvium from CPP-31: vadose zone concentrations (vertical contours) (pCi/L) (MCL = thick red line, 10*MCL = thin red line, MCL/10 = black line).

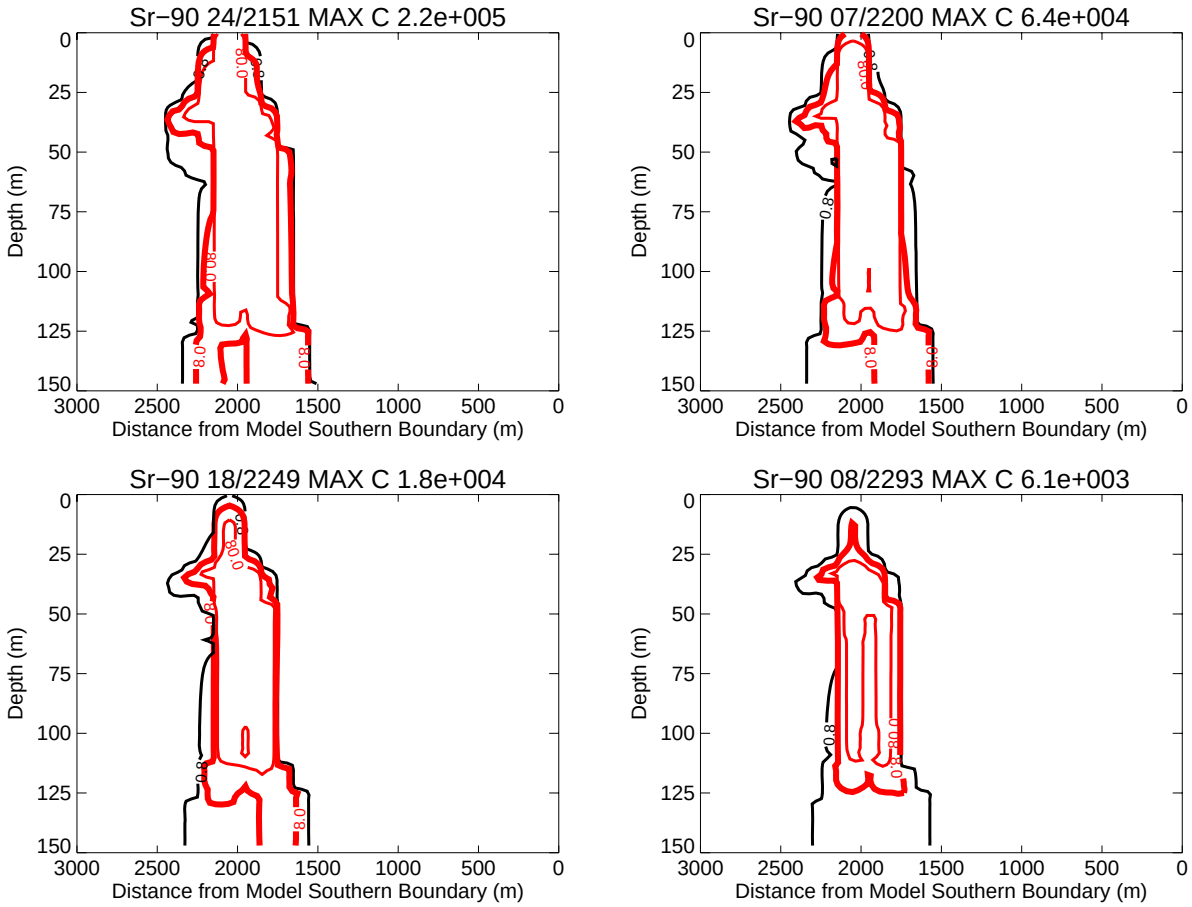

Figure J-9-31. Sr-90 remaining in the alluvium from CPP-31:vadose zone concentrations (vertical contours) (pCi/L) (continued) (MCL = thick red line, 10*MCL = thin red line, MCL/10 = black line).

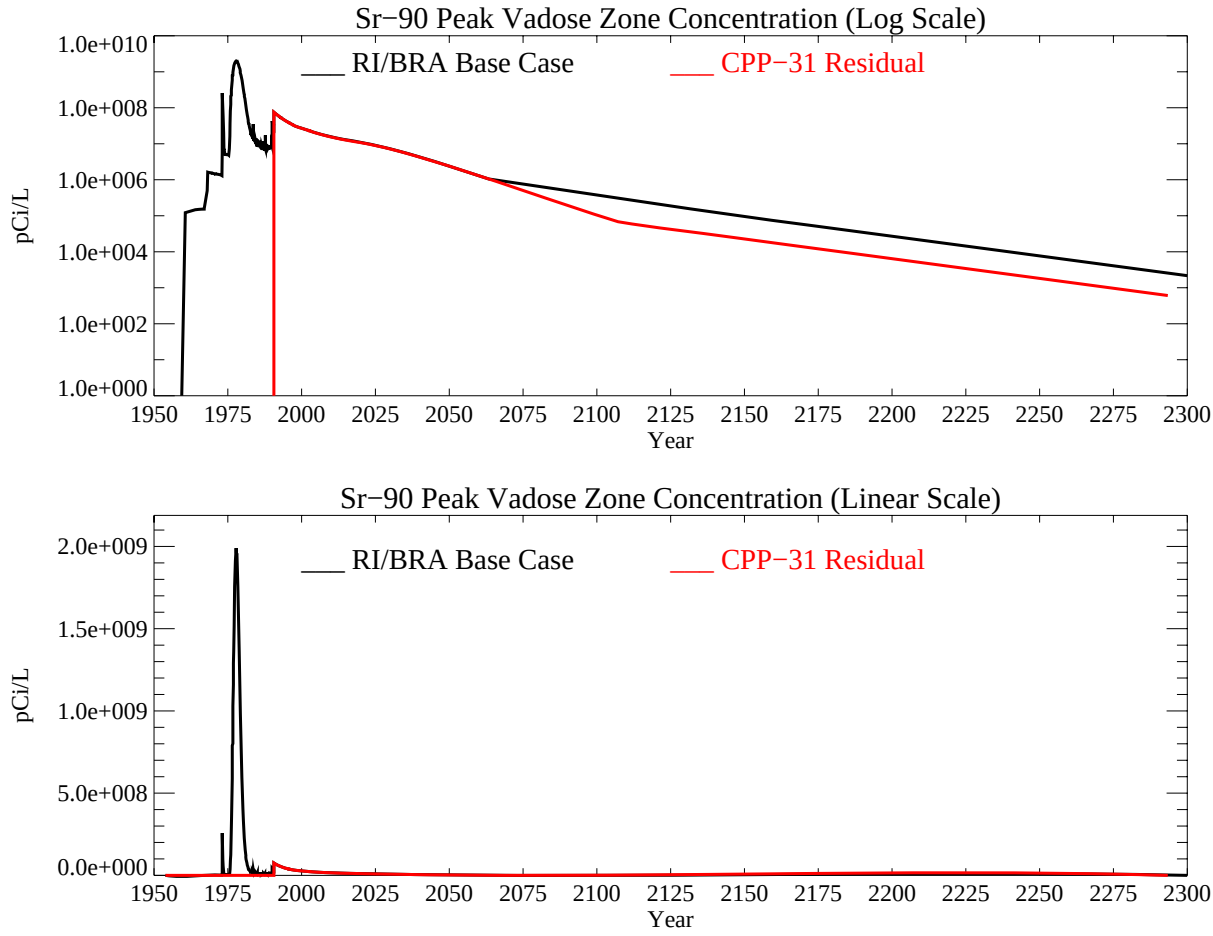

Figure J-9-32. Sr-90 remaining in the alluvium from CPP-31: peak vadose zone concentrations (pCi/L) with the RI/BRA model in black and this residual after 20 years from CPP-31 in red.

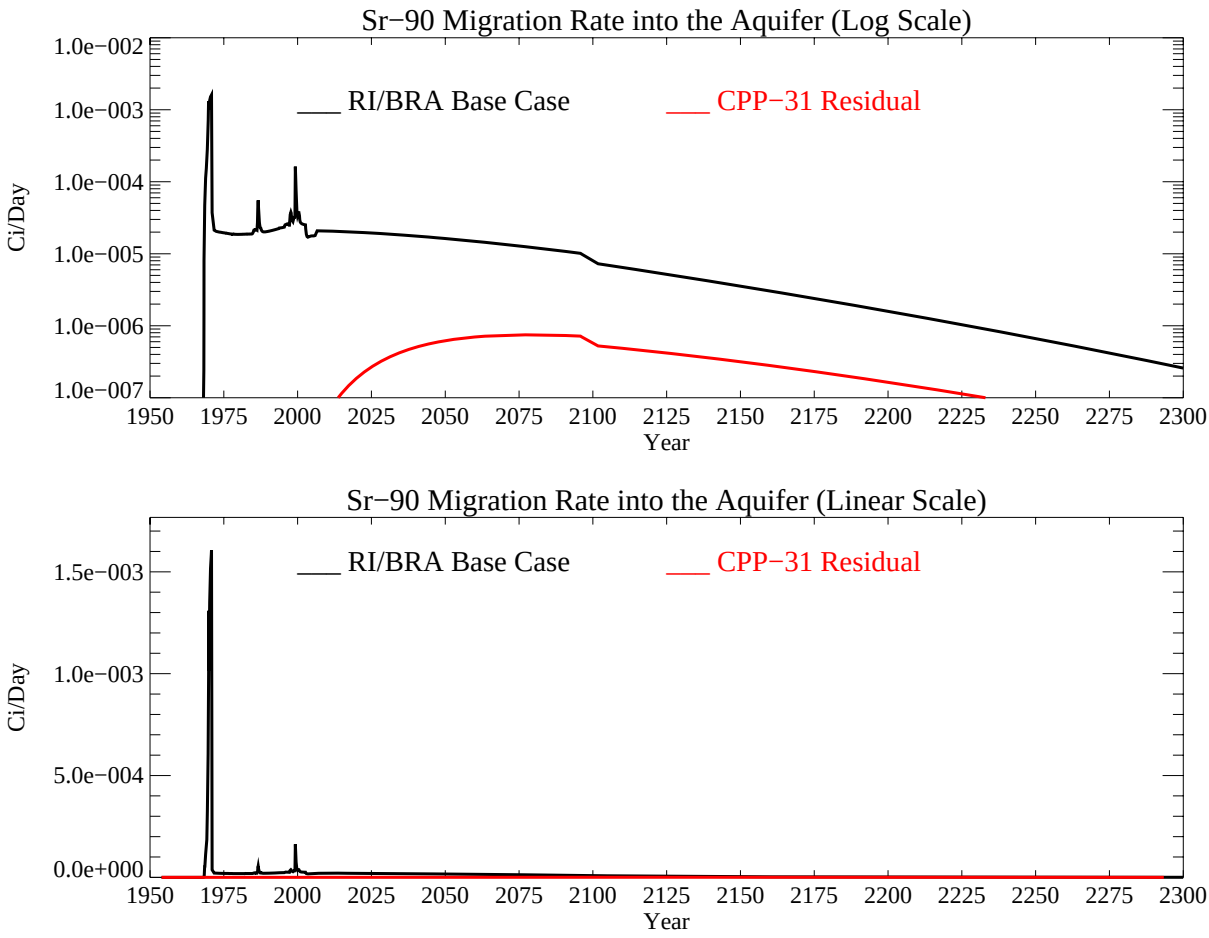

Figure J-9-33. Sr-90 remaining in the alluvium from CPP-31: activity flux into the aquifer (Ci/day) with the RI/BRA base case in black, and the CPP-31 residual in red.

J-9.4.2 Aquifer Sr-90 Simulation Results

The resultant peak aquifer concentration is given in Figure J-9-34. The highest predicted concentration from the CPP-31 residual source is 1.77 pCi/L, which occurs in year 2077. The predicted concentration in year 2095 is just slightly lower at 1.7 pCi/L. Concentrations are less than 1 pCi/L from this residual alluvial source after year 2110. On this figure, the peak concentration resulting from all source of Sr-90 is shown in black for the RI/BRA base simulation using these same model parameters. During the 2030 to 2150 time period, the peak concentration from all of the sources of Sr-90 exceeds 25 pCi/L. This means that less than 10% of the total is being supplied by the 3564 Ci of Sr-90 remaining in the alluvium after 1993.

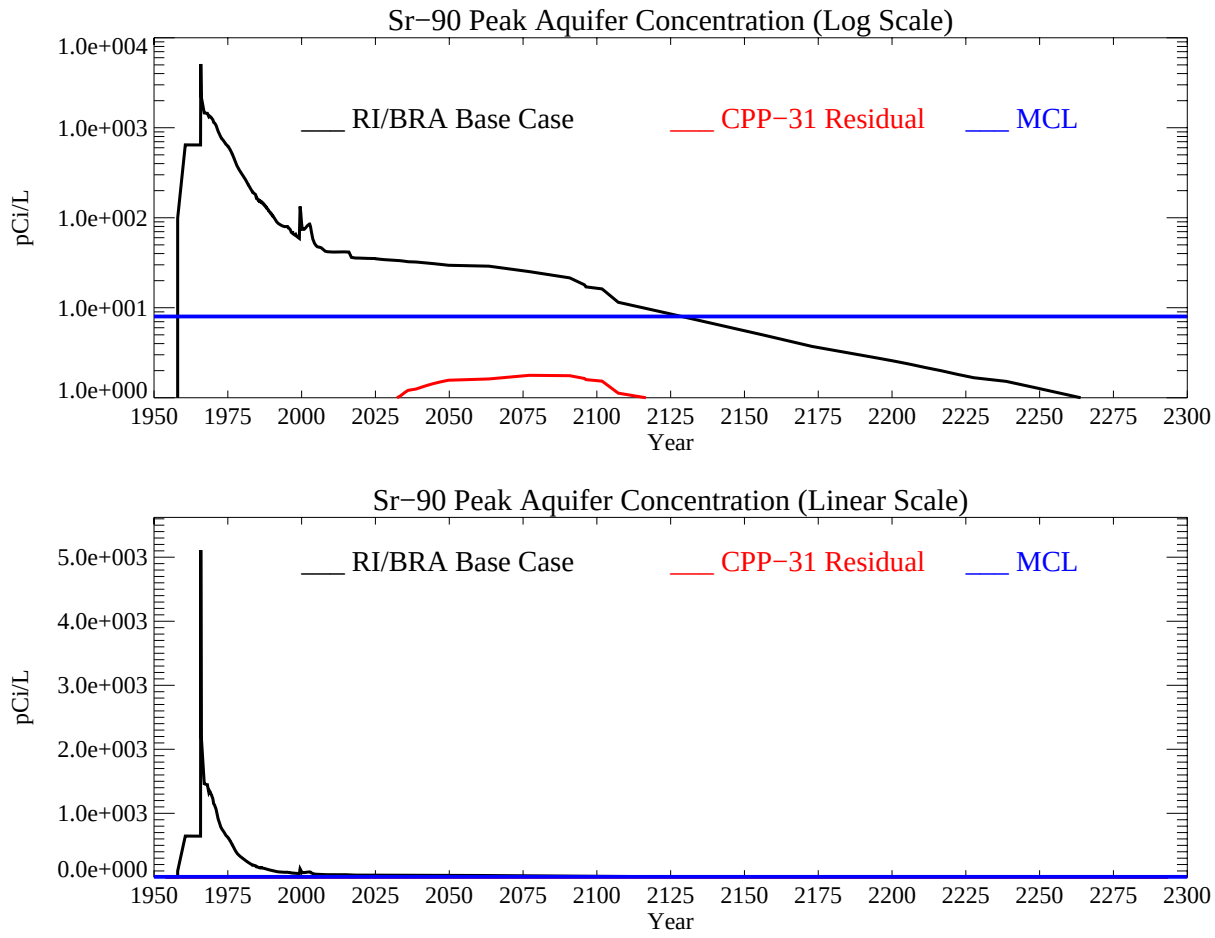

Figure J-9-34. Sr-90 remaining in the alluvium from CPP-31: peak aquifer concentrations (pCi/L) with the MCL in blue, RI/BRA model in black and this residual from CPP-31in red.

J-10 SENSITIVITY TO GEOCHEMICAL INPUTS

Primary geochemical parameters include alluvium properties: cation exchange capacity, selectivity coefficient for strontium, and background sodium concentration; and interbed K_d. Sensitivity to the cation exchange capacity and selectivity coefficients were determined through simulation using the base model discussed in Section J-8. In the following simulations a single parameter change was made. The simulation forming the basis of the sensitivity simulations used a CEC of 2 meq/100 g, a strontium selectivity coefficient of 0.35, a background sodium concentration of 3.3 mmol/L, and an interbed K_d of 22 mL/g. The sensitivity to cation exchange capacity includes simulations using a CEC of 3 meq/100 g, 5 meq/100 g, or 7 meq/100 g. The sensitivity to strontium selectivity coefficient ($K_{Na/Sr}$) used a range from 0.25 to 0.45. Sensitivity to background sodium concentration evaluated the effect of lowering pore water sodium concentrations to 0.22 mmol/L. Sensitivity to interbed K_d was also assessed, by raising the K_d from 22 mL/g to 78 mL/g (spanning the entire range). To assess model sensitivity, we have chosen to look at 1) total activity leaving the alluvium at periods of 5, 10, 15, and 20 yrs, 2) effective adsorption capacity (K_d) after 20 yrs, 3) the impact on the vadose zone, and 4) resultant aquifer concentrations. These results are summarized following the presentation of all simulation in Table J-10-1.

J-10.1 Alluvial CEC of 3 meq/100 g

The recommended CEC range for INTEC alluvial material is 2-8 meq/100 g. A value of 2 meq/100 g was used in the RI/BRA model, and a value of 3 meq/100 g is evaluated here. This simulation uses an infiltration rate from precipitation of 18 cm/yr applied across the INTEC facility, all of the anthropogenic water, and an interbed of K_d=50 mL/g as was used in the RI/BRA base case (Section J-8).

J-10.1.1 Geochemical Evolution in the Alluvium

Summary performance measures for the geochemical evolution of Sr-90 in the alluvium are presented in Figure J-10-1 and can be compared to the RI/BRA base case measures shown in Figure J-8-9. An increase from 2 meq/100 g to 3 meq/100 g has increased the amount of Sr-90 associated with the solid phase as shown by the amount of Sr-90 on exchange sites (subplot I) The total curies after 20 years adsorbed with a CEC of 2 meq/100 g is roughly 3500, compared to nearly 5000 in this scenario. As more of the Sr-90 is associated with exchange sites, it is removed from the aqueous solution. Subplots A-F show the significant decrease in SrNO3 and Sr+ ion, SrCO3, and SroH in the aqueous phase.

The relative abundance of SrNO3 is much larger than the other species, and a 5% decrease is significant. It results in only 10864 Ci leaving the alluvium relative to the 12336 Ci predicted in the RI/BRA base case. After 5, 10, 15, and 20 years, the total Sr-90 that has entered the vadose zone under the alluvium is 14239, 10820, 10842, and 10864 Curies, respectively as shown in Figure J-10-1-G. With this higher CEC, a larger fraction (5036 Ci vs. 3564 Ci) remains in the alluvium after 20 years (Figure J-10-1-I).

The largest difference in the distribution of Sr-90, relative to the base case, occurs in the adsorbed Sr-90. The effective K_d is essentially the ratio of activity on the exchange sites to that in the aqueous phase. As the exchanged activity increases, the aqueous phase Sr-90 concentrations decrease, and the effective K_d increases. The time evolution of this parameter is quite different than observed in the RI/BRA base case (Figure J-10-1 (J)). During the 7-15 year period, the effective K_d is almost double that in the RI/BRA base case. After 20 years, the effective K_d is approaching an average value of 3.75 mL/g.

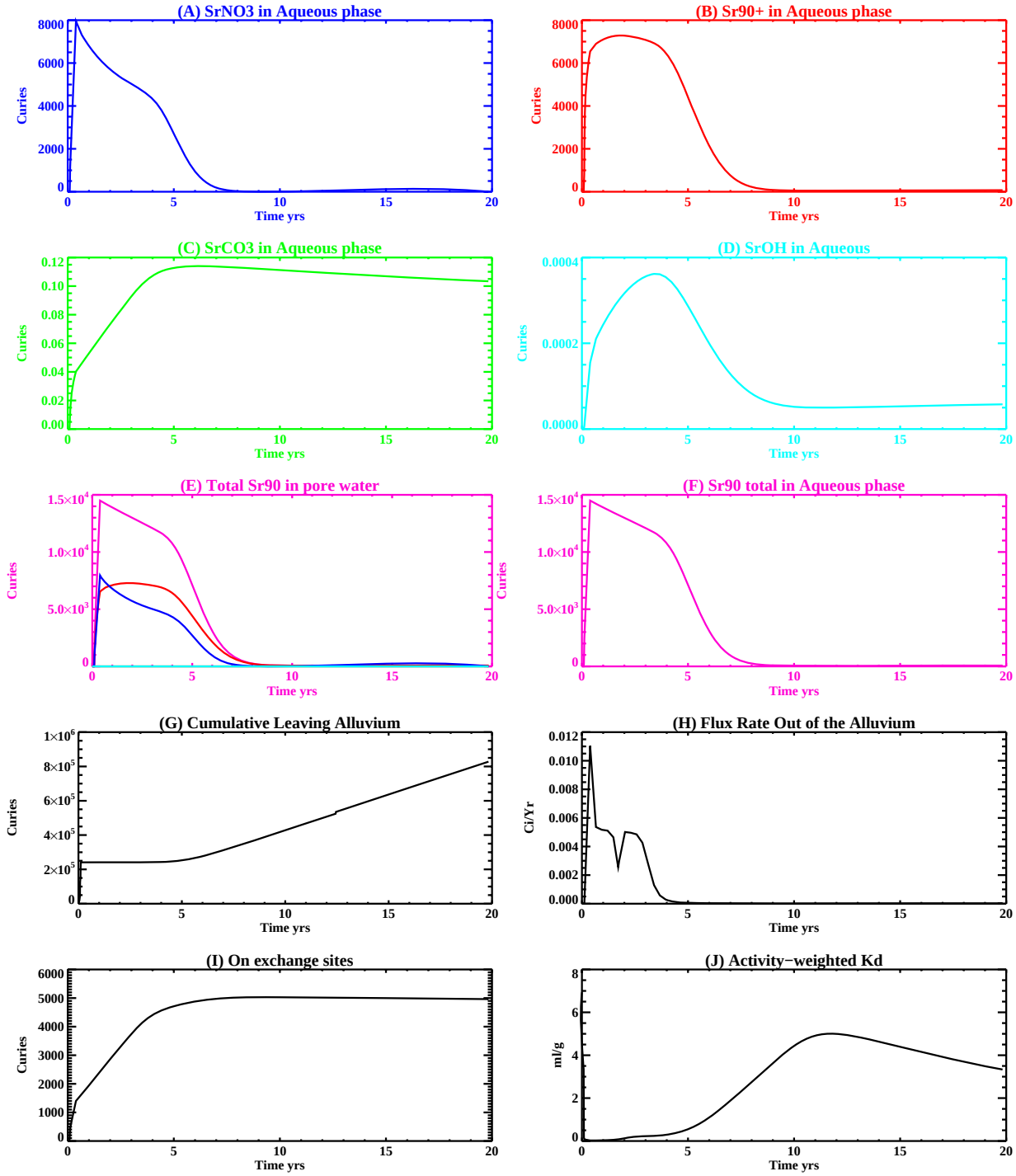

Figure J-10-1. Summary figure illustrating the speciation of Sr-90 in the aqueous phase (A-F), total Sr-90 in the pore-water of the alluvium (E), cumulative curies of Sr-90 having left the alluvium (G), flux rate leaving the alluvium (H), Sr-90 on the exchange sites (I), and effective partitioning coefficient (Kd) (J).

J-10.1.2 Vadose Zone Sr-90 Simulation Results

The release of Sr-90 in this simulation followed the same procedure as was used in the RI/BRA model:

- 15900 Ci from CPP-31 release in the tank farm were represented using (a) the activity-release function shown in Figure J-10-1 (H) for the 10864 Ci released during the first 20 years, and placing this activity flux directly above the basalt interface of the base model (Appendix A, Section 5.1); and (b) distributing the remaining 5036 Ci through the alluvium scaled to the measured soil concentrations obtained during the 2004 sampling cycle (Appendix G and Table 5-32). To simulate the transport of the activity remaining in the alluvium, an effective K_d of 3.75 mL/g was used (Figure J-10-1 (J)) for the alluvium sediments.
- transport of Sr-90 from sources other than CPP-31 originating in the alluvium, whose location is spanned by the submodel (Appendix A, Section 5.1), were simulated using the submodel. Because these source locations were outside the influence of the high ionic strength, acidic CPP-31 release, a K_d of 20 mL/g was used in the submodel alluvium.
- transport of Sr-90 from sources located outside of the submodel horizontal extent were also placed in the base model used to simulate the transport of the CPP-31 remaining in the alluvium. The effective K_d for the alluvium underlying these source locations was also set to the value used to simulate the transport of Sr-90 predicted to remain in the alluvium after 20 yrs (first bullet). The relative magnitude of these sources are small relative to the residual Sr-90 predicted to remain in the alluvium after 20 yrs. In this case, the K_d is much smaller than that used to simulate the transport of Sr-90 from sources within the submodel boundary. This conservativism might increase peak aquifer concentrations slightly.

The horizontal and vertical distribution of Sr-90 in the vadose zone is given in Figures J-10-2 through J-10-5 through the year 2293. Primarily because of the contour intervals provided (plus/minus one order of magnitude of the MCL), the differences relative to the RI/BRA base case are imperceptible in these figures.

One of the goals of this sensitivity study is to explain the choice of RI/BRA model, which is best accomplished by comparing the available field data to model predictions. The arrival of Sr-90 in key perched water wells is shown in Figure J-10-6 and is summarized by the RMS error for all perched water wells in Figure J-10-7. In this simulation, about 90% as much Sr-90 was initially released into the perched water relative to the RI/BRA base case, and the Sr-90 remaining in the alluvium will not have arrived to influence these calibration measures. Because of the timing, these results can be compared to the RI/BRA base case (Figures J-8-14 and J-8-15). In the RI/BRA base case, the model was overpredicting concentrations in northern perched water wells. By releasing less Sr-90 into the perched water, this model matches the data slightly better, but the differences are small. In southern INTEC, predicted concentrations in this case are slightly better. However, concentrations in the southern INTEC wells are orders of magnitude smaller than they are in northern INTEC. Bettering the match to those wells at the expense of a worse match in northern INTEC is not desirable. Overall, the relatively small difference in Sr-90 released into the perched water results in very similar perched water concentrations and very similar matches to the field data. A detailed comparison of the model fit to field data for both of these primary model parameter sets is presented in Section J-12 following the remainder of the sensitivity results. This similarity is reflected in the peak vadose zone concentrations through time presented in Figure J-10-8.

The rate at which Sr-90 enters the aquifer is given in Figure J-10-9, and can be compared directly to the RI/BRA model (black) results. Nearly doubling the amount of Sr-90 arriving in the perched water within the first 20 years following the CPP-31 release has not resulted in a commensurate increase in flux rate out of the vadose zone.

Figure J-10-2. Sr-90 vadose zone concentration assuming an alluvium CEC=3 meq/100 g (horizontal contours) (pCi/L) (MCL = thick red line, 10*MCL = thin red line, MCL/10 = black line).

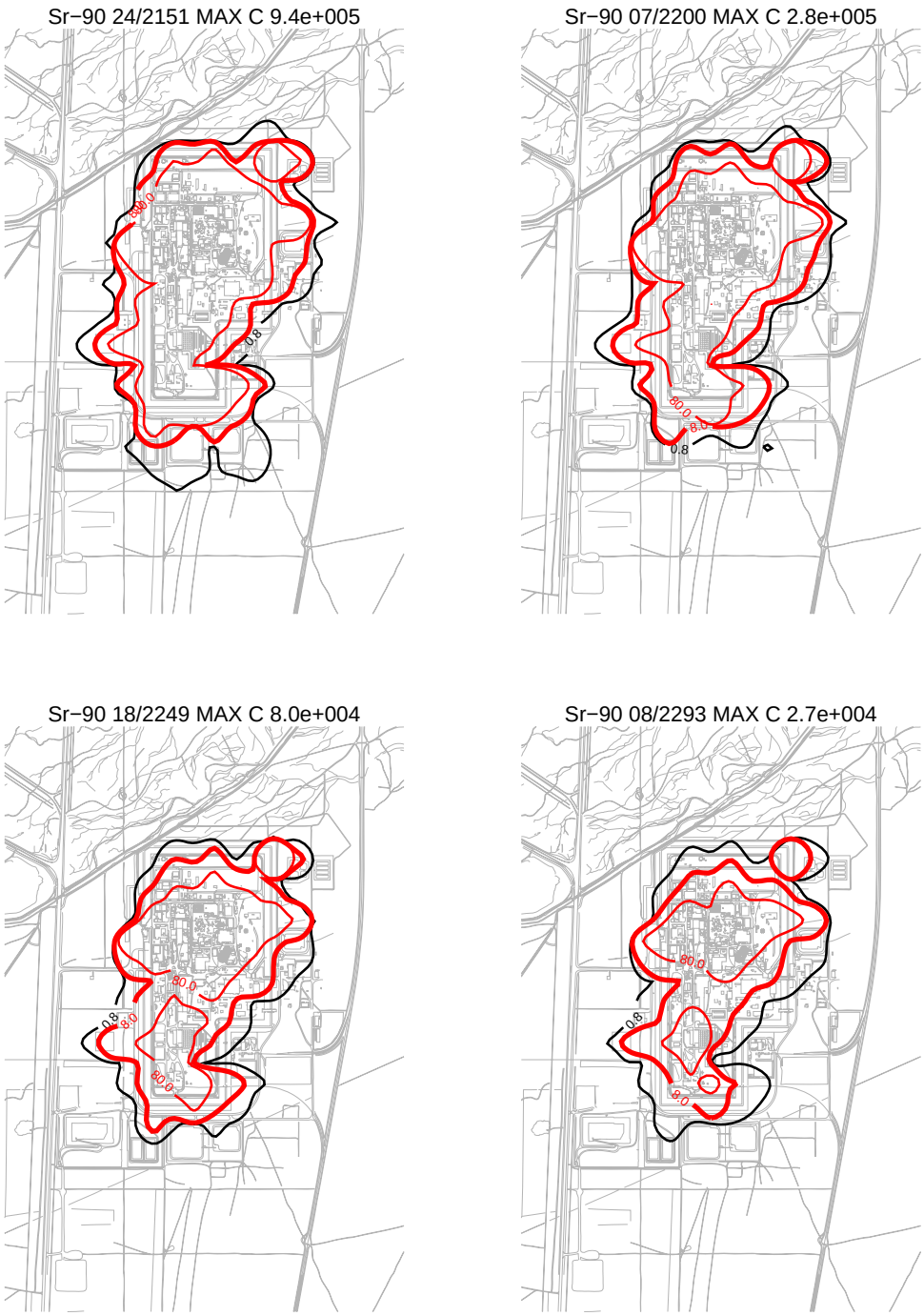

Figure J-10-3. Sr-90 vadose zone concentration assuming an alluvium CEC=3 meq/100 g (horizontal contours) (pCi/L) (MCL = thick red line, 10*MCL = thin red line, MCL/10 = black line).

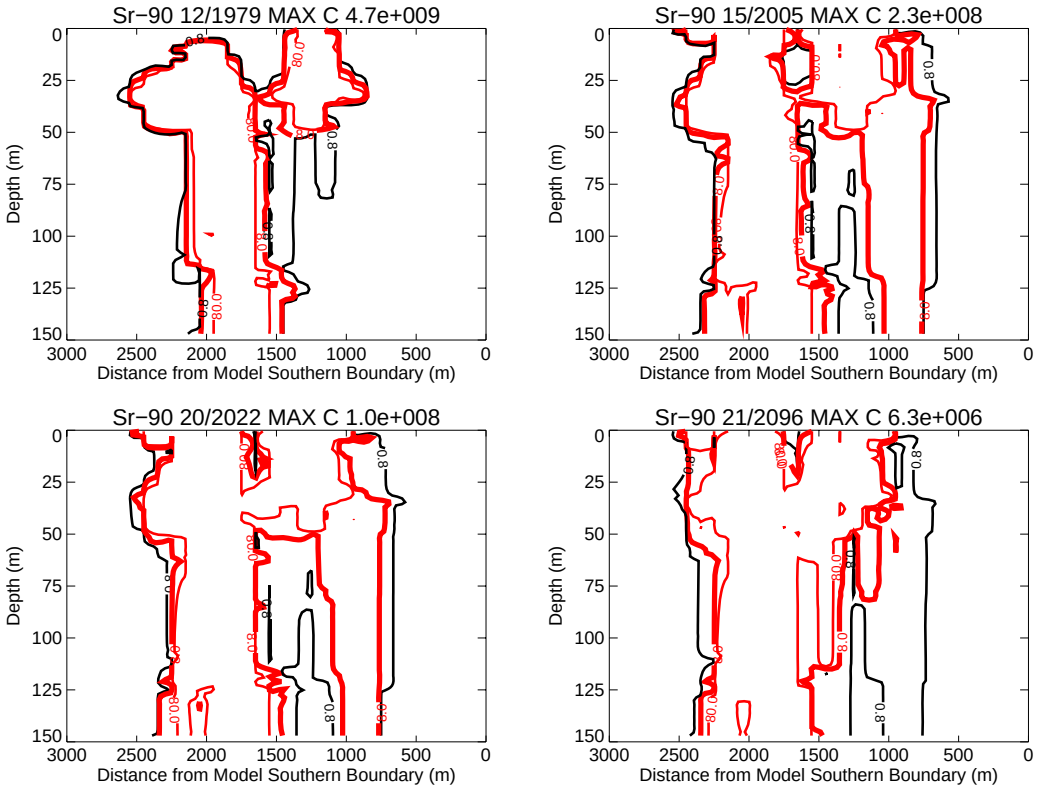

Figure J-10-4. Sr-90 vadose zone concentrations assuming an alluvium CEC=3 meq/100 g (vertical contours) (pCi/L) (MCL = thick red line, 10*MCL = thin red line, MCL/10 = black line).

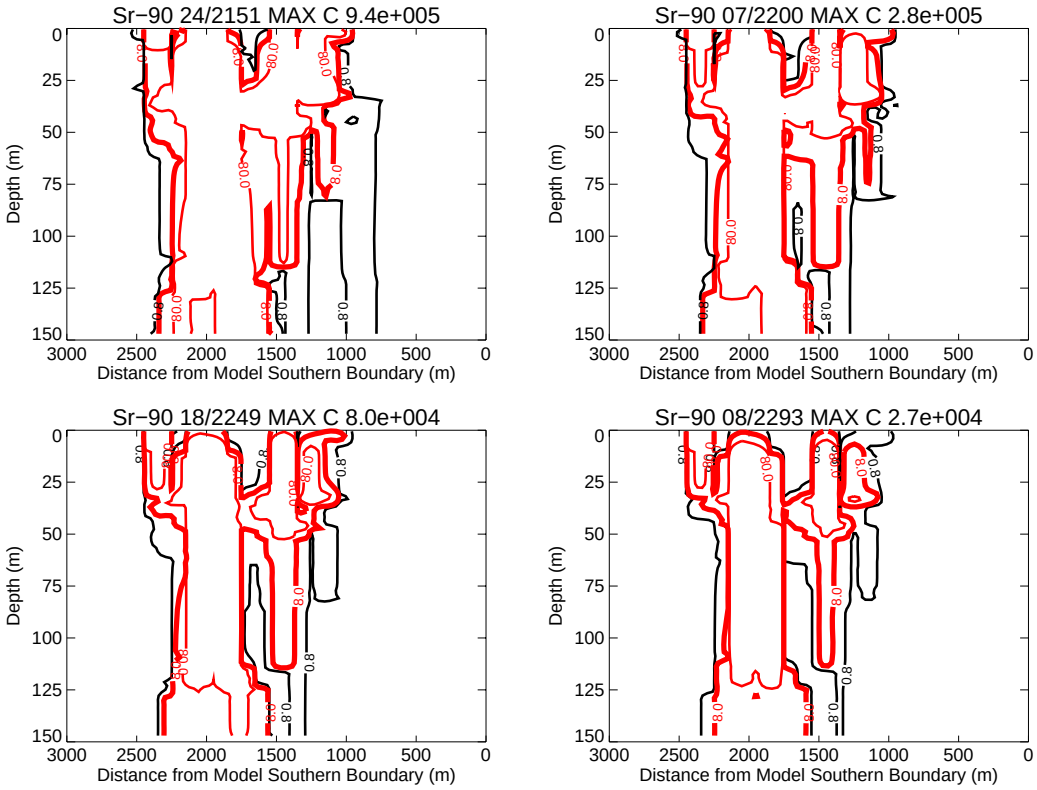

Figure J-10-5. Sr-90 vadose zone concentrations assuming an alluvium CEC=3 meq/100 g (vertical contours) (pCi/L) (continued) (MCL = thick red line, 10*MCL = thin red line, MCL/10 = black line).

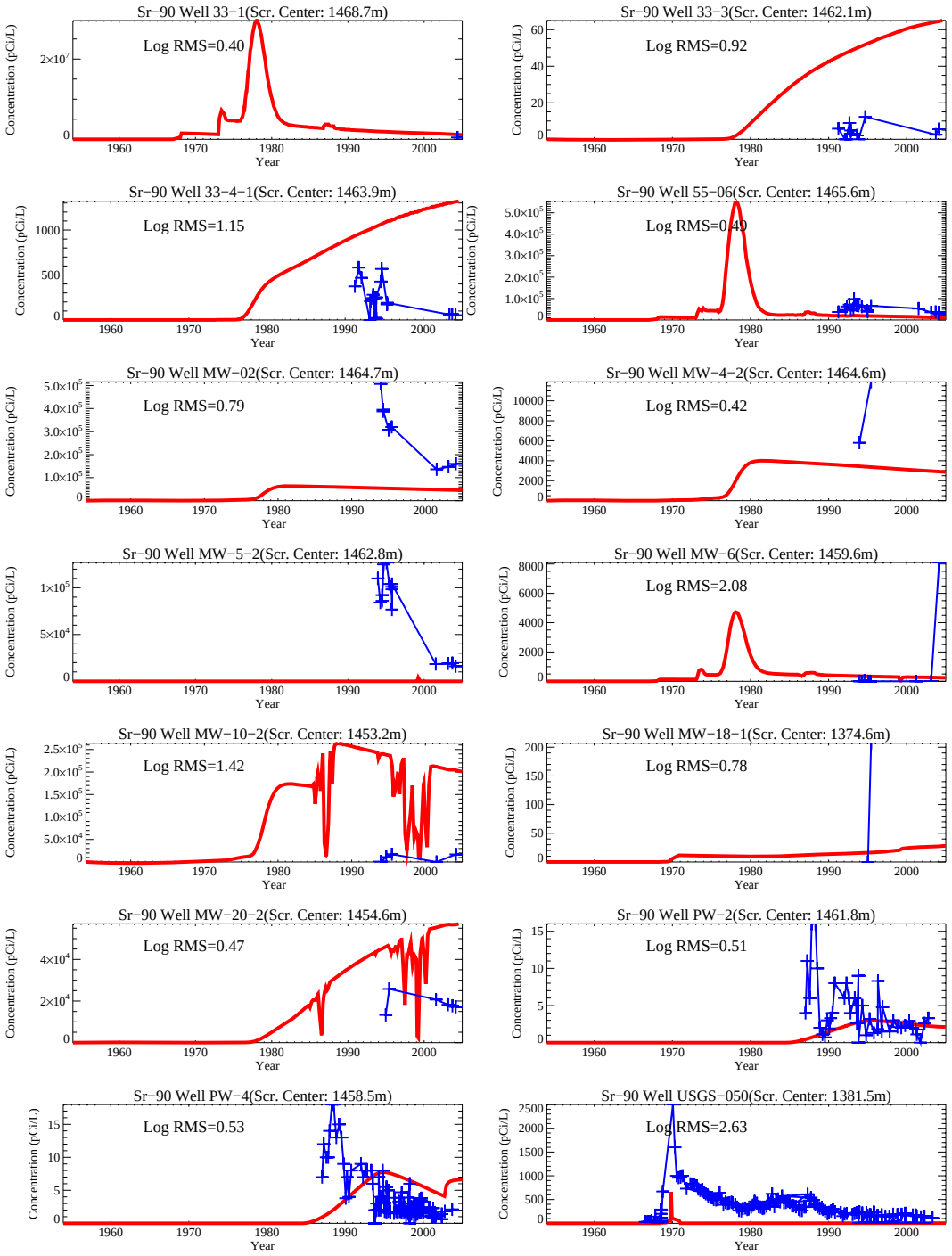

Figure J-10-6. Sr-90 concentration in perched water wells assuming an alluvium CEC=3 meq/100 g (pCi/L) (Measured values = blue crosses, red = model at screen center).

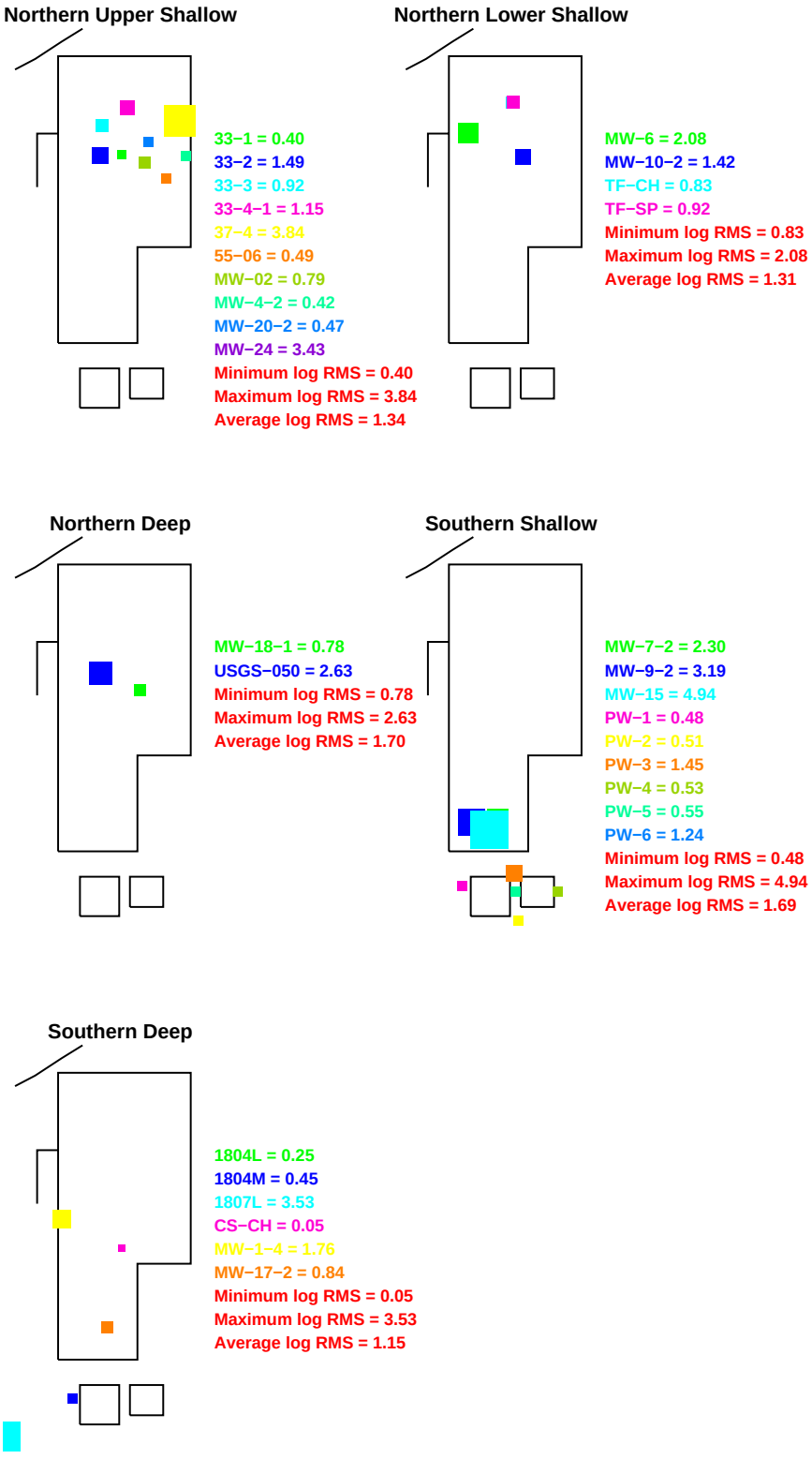

Figure J-10-7. Log 10 Root mean square error (RMS) by depth and northing assuming an alluvium CEC=3 meq/100 g.

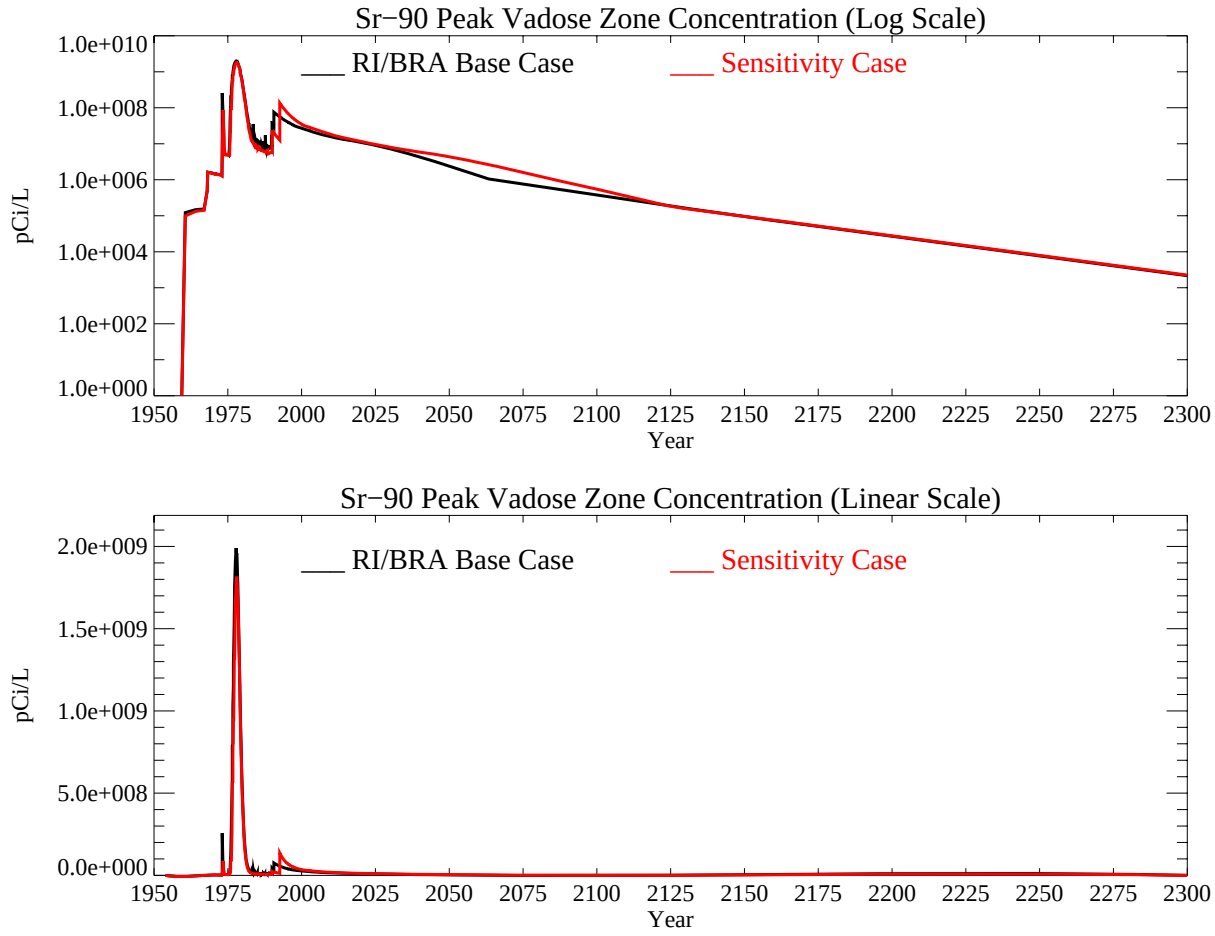

Figure J-10-8. Sr-90 peak vadose zone concentrations assuming an alluvium CEC=3 meq/100 g (pCi/L) with the RI/BRA model in black and this sensitivity run in red.

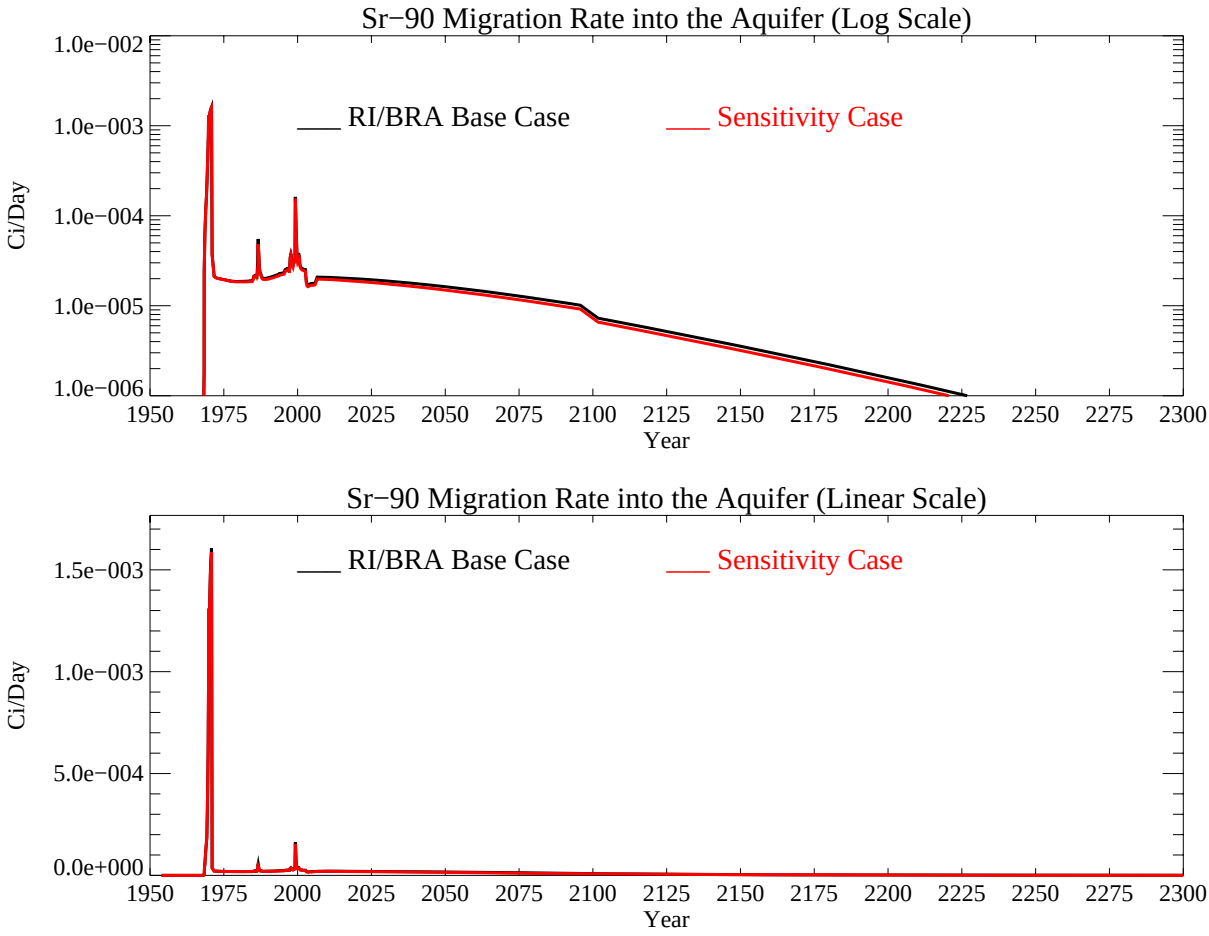

Figure J-10-9. Sr-90 activity flux into the aquifer assuming an alluvium CEC=3 meq/100 g (Ci/day) with the RI/BRA model in black, and this sensitivity run in red.

J-10.1.3 Aquifer Sr-90 Simulation Results

The distribution of Sr-90 in the aquifer for the time period spanning 2005-2096 on the course grid is given in Figure J-10-10. It is presented for the 2049-2151 time period on the fine grid in Figure J-10-11. Resultant peak aquifer concentrations are given in Figure J-10-12, with the red line representing the results of this simulation. Because the Sr-90 originating at land surface does not arrive in the aquifer until the late 1980's, comparisons to measured data are not presented for aquifer wells.

The three important performance measures are concentrations beyond 2095, the spatial extent of contamination, and the time period during which concentrations exceed the MCL. The predicted peak Sr-90 concentration in the year 2095 is 16.7 pCi/L, about 90% of that predicted in the RI/BRA model. This is in direct proportion to the amount of Sr-90 arriving in the perched water within 20 years of the CPP-31 release. This concentration is twice as high as the MCL. The peak concentration in year 2095 is insignificantly different from the RI/BRA base case compared to the overall model uncertainty.

The Sr-90 contour plots presented in Figures J-10-10 and J-10-11 illustrate that the predicted distribution in the aquifer does not differ greatly from that predicted in the RI/BRA model. They show that although concentrations are predicted to exceed the MCL beyond 2095, that the area impacted by Sr-90 above 8 pCi/L is between the INTEC fence and the former percolation ponds in 2095.

The third measure in this sensitivity result is the time during which the MCL is exceeded. A 20% reduction in the amount of Sr-90 released from the alluvium into the perched water allows the MCL to be reached only 6 years earlier than predicted in the RI/BRA base case. In this case, the simulated Sr-90 concentrations remain above the MCL from 1960 through year 2123, while in the RI/BRA base case it occurred by year 2129. Given the overall model uncertainty, this difference is insignificant.

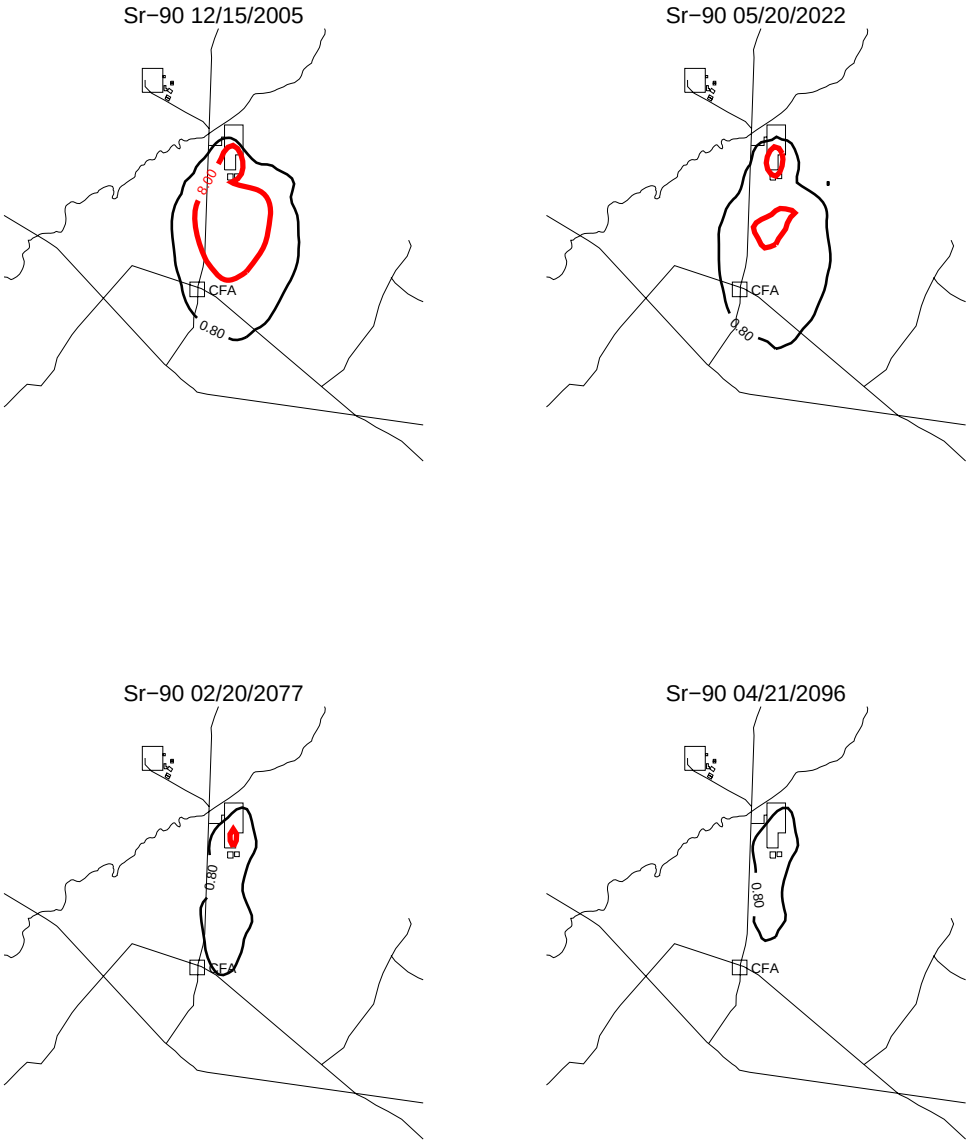

Figure J-10-10. Sr-90 aquifer concentration contours assuming an alluvium CEC=3 meq/100 g (pCi/L) (MCL = thick red line, 10*MCL = thin red line, MCL/10 = black line).

Figure J-10-11. Sr-90 aquifer concentration contours assuming an alluvium CEC=3 meq/100 g (pCi/L) (continued) (MCL = thick red line, 10*MCL = thin red line, MCL/10 = black line).

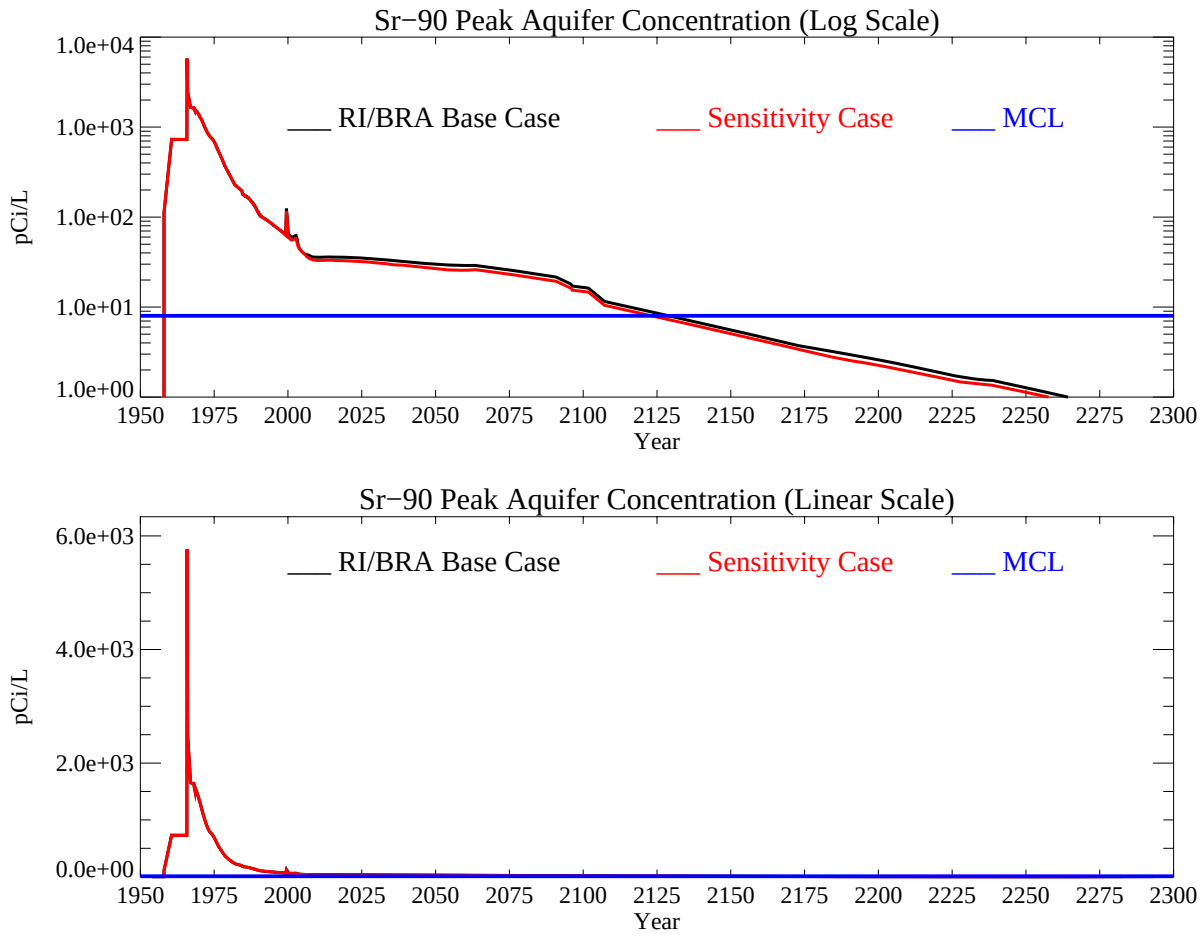

Figure J-10-12. Sr-90 peak aquifer concentrations assuming an alluvium CEC=3 meq/100 g (pCi/L) with the MCL in blue, RI/BRA model in black and this sensitivity run in red.